Shared Aperture Metasurface Antennas for Multibeam Patterns

David Gonzalez-Ovejero[1], Gabriele Minatti[2], Enrica Martini[2,3], Goutam Chattopadhyay[1], and Stefano Maci[2]
[1] Jet Propulsion Laboratory, California Institute of Technology, Pasadena, CA 91109, USA, david.gonzalez@jpl.nasa.gov
[2] Dept. of Information Engineering and Mathematics, 53100 Siena, Italy, macis@diism.unisi.it
[3] Wave Up S.r.l., Florence 50126, Italy,

***Abstract*—This paper describes various possibilities for designing multibeam antennas using a single metasurface (MTS) aperture. Both single-source and multi-source feeding schemes are considered. For the single-source case, two approaches are investigated: i) division of the aperture in several angular sectors (one per beam) and ii) superposition of the individual modulations required to obtain the beams in the desired directions. A configuration based on a multi-source feeding scheme is also tailored by a superposition of modulation patterns. Numerical results based on the Method of Moments are presented for validation.**

***Index Terms*—Metasurface antennas, multibeam antennas, antenna efficiency, leaky waves.**

I. Introduction

Modulated metasurface (MTS) antennas have undergone an unprecedented development in recent years [1]-[5]. Their main advantages are the low-profile, light-weight and efficient control of the aperture fields, which make them attractive for deep space communications in the microwave range [2], and for science instruments at submillimeter-waves [5]. However, to date, only a handful of works [6]-[7] have treated the problem of obtaining multiple beams with a single MTS aperture. Previous works have used isotropic surface impedances, which present a low aperture efficiency, owing to the high level of cross polarized fields [2]. Indeed, [7] is more focused on beam frequency scanning than on aperture efficiency. Since the aperture efficiency is a key parameter in many applications, we use here an anisotropic impedance instead. This paper builds on the results obtained in [2] and [4] to study the generation of multiple beams using either a single source or multiple sources. An added value to the presented approach is the control of the aperture fields' amplitude such that the aperture efficiency is high.

Radiation by MTS antennas stems from the interaction of a cylindrical surface-wave (SW), excited by a point source, with a periodically modulated Impedance Boundary Condition (IBC). The periodic modulation is tailored in such a way that the (-1) indexed Floquet mode falls into the visible region, thus becoming a leaky-wave. The modulation is achieved by changing the shape and orientation of sub-wavelength patches, printed on a grounded slab (plane $z = 0$) with relative permittivity ε_r and thickness h (see Fig. 1a). In the following, we will represent the cladding as a sheet transition IBC [8],[9] given by $\underline{\underline{\mathbf{X}}}$ as:

$$\mathbf{E}_t = j\underline{\underline{\mathbf{X}}} \cdot \hat{\mathbf{z}} \times \left(\mathbf{H}_t\big|_{z=0^+} - \mathbf{H}_t\big|_{z=0^-} \right) = j\underline{\underline{\mathbf{X}}} \cdot \mathbf{J} \qquad (1)$$

where $\mathbf{J}$ represents the difference in the tangential components of the H-field on either side of the MTS, and it can be viewed as the current flowing in the cladding. $\mathbf{E}_t$ is the average of the E-field on either side of the MTS. Under certain assumptions of symmetry in the patches' shape and in absence of losses, $\underline{\underline{\mathbf{X}}}$ is a Hermitian tensor [10].

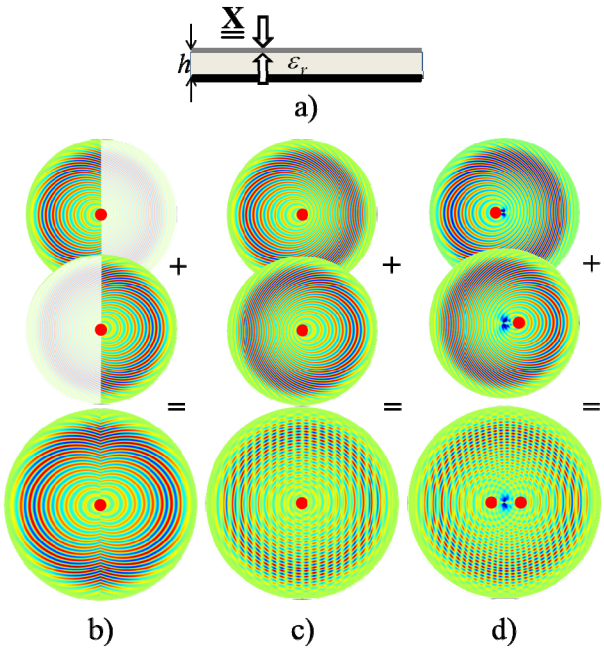

Fig. 1. (a): Reference structure composed of a grounded dielectric slab, printed with sub-wavelength metal patches. (b)-(d) $X_{\rho\rho}$ component of the surface reactance tensor of MTS apertures which provide two beams. Three solutions are presented: (b) single source with partition of the aperture in 2 sectors; (c) single source with aperture sharing by a superposition of modulated impedance patterns, and (d) two sources with aperture sharing by a superposition of modulated impedance patterns.

In the next section, we provide closed-form expressions of $\underline{\underline{\mathbf{X}}}$ to obtain multibeam operation. Such sheet transition IBCs can be easily implemented by means of sub-

wavelength elliptical patches printed on a grounded slab. To this end, one can apply the procedure described in [4], which is based on the discretization of the antenna aperture in sub-wavelength square cells, and a local periodicity approximation. The extraction of the patch parameters that correspond to each local value of the reactance tensor is carried out using the method in [11]. The expressions in [11] allow us to efficiently create a data base that relates the transparent IBC values with the major axis of the elliptical patch, its eccentricity, and its rotation angle inside the cell. Then, for each cell, a best fitting process is carried out in order to obtain the dimension and orientation of the patches that correspond to the theoretical values of $\underline{\underline{\mathbf{X}}}$. In the following, we will show only results that correspond to the simulation of $\underline{\underline{\mathbf{X}}}$ with the method of moments (MoM) tool described in [12]. This is possible owing to the excellent agreement shown in [12]-[13] between the simulations of continuous sheet transition IBCs and the simulations of actual structures.

II. Multibeam Metasurface Antennas

Multiple beams will be obtained with a single MTS aperture by means of three different configurations, schematically shown in Fig. 1(b)-(d). The proposed architectures are:

A). Single source with aperture partition in angular sectors.
B). Single source with superposition of impedance modulation.
C). Multi-source with superposition of impedance modulations.

In cases A) and B), a single vertical electric dipole (VED) at the center of the aperture (red dots in Fig. 1) and on the MTS plane is used to create multiple beams simultaneously. Conversely, in case C) we have several VED sources in different positions, which are used to excite different independent beams. We will limit the analysis in this paper to the case of two right-handed circularly polarized (RHCP) beams. More general cases can be found in [13]. All the examples present a 12λ aperture radius, with λ being the wavelength, at 26.5 GHz, and have been designed for a substrate with ε_r=9.8 and h=0.508 mm. The surface impedance patterns required to obtain two beams with solutions A), B) and C), are shown in Fig. 1(b), (c), and (d), respectively. We will denote the direction of each beam by

$$\hat{\mathbf{r}}_n = \sin\theta_0\cos\varphi_n\hat{\mathbf{x}} + \sin\theta_0\sin\varphi_n\hat{\mathbf{y}} + \cos\theta_0\hat{\mathbf{z}} \qquad (2)$$

where n=1, 2, $\theta_0 = 30°$, and $\varphi_1 = 0, \varphi_2 = \pi$. In turn, $\boldsymbol{\rho}$ will be the observation point on the MTS plane, described in cylindrical coordinates (ρ,φ), and with unit vector $(\hat{\boldsymbol{\rho}},\hat{\boldsymbol{\varphi}})$. Now, the (-1) term of the Floquet-wave expansion, which provides the tangential electric field in the aperture plane, can be written as:

$$\mathbf{E}^{(-1)}(\boldsymbol{\rho}) = \sum_{n=1}^{2}\mathbf{e}_n\, E_0 e^{-\mathrm{j}k\,\hat{\mathbf{r}}_n\cdot\boldsymbol{\rho}} e(\rho) U_n U_A \qquad (3)$$

where $\mathbf{e}_1$=$\hat{\mathbf{x}}\cos\theta_0 + j\,\hat{\mathbf{y}}$, $\mathbf{e}_2 = -\hat{\mathbf{x}}\cos\theta_0 - j\,\hat{\mathbf{y}}$, and k is the free space wavenumber.

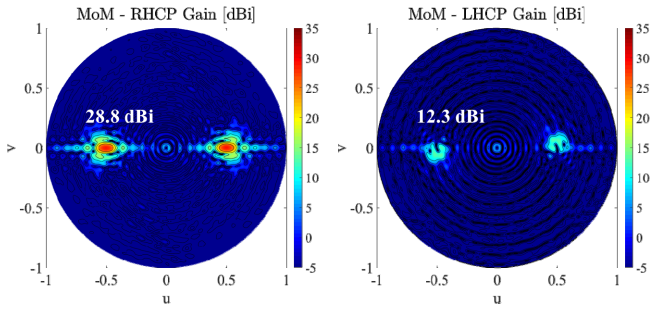

Fig. 2. (a) RHCP and (b) LHCP gains in the u-v plane for the reactance tensor given by (4).

A. Case A): single point source with aperture partition

The design method in [4] is adopted to provide two beams by writing the tensor surface reactance as the sum of 2 angular sectors

$$\underline{\underline{\mathbf{X}}} = \sum_{n=1}^{2}\left[\hat{\boldsymbol{\rho}}\hat{\boldsymbol{\rho}}\,X_{\rho\rho}^{(n)} + \left(\hat{\boldsymbol{\rho}}\hat{\boldsymbol{\varphi}}+\hat{\boldsymbol{\varphi}}\hat{\boldsymbol{\rho}}\right)X_{\rho\varphi}^{(n)} + \hat{\boldsymbol{\varphi}}\hat{\boldsymbol{\varphi}}\,X_{\varphi\varphi}^{(n)}\right]U_n U_A \quad (4)$$

where $U_A = u(a-\rho)$, with $u(x)$ being the unit step function, and $U_n(\varphi)$ represents each of the two sectors which result from dividing the aperture along the y axis. The functions U_n provide the partition in angular sectors. In addition, the tensor elements for sector n will be modulated to provide a beam in direction $\hat{\mathbf{r}}_n$. Such modulation can be written as

$$\begin{aligned}
X_{\rho\rho}^{(n)}(\boldsymbol{\rho}) &= \mathrm{X}_0\left[1 + m_\rho^{(n)}(\rho)\sin\left(\beta_{sw}\rho - k\,\hat{\mathbf{r}}_n\cdot\boldsymbol{\rho} + \Phi_\rho^{(n)}\right)\right]\\
X_{\rho\varphi}^{(n)}(\boldsymbol{\rho}) &= \mathrm{X}_0\, m_\varphi^{(n)}(\rho)\sin\left(\beta_{sw}\rho - k\,\hat{\mathbf{r}}_n\cdot\boldsymbol{\rho} + \Phi_\varphi^{(n)}\right)\\
X_{\varphi\varphi}^{(n)} &= \frac{\mathrm{X}_0}{\left|\mathbf{e}_n\cdot\hat{\boldsymbol{\rho}}\right|^2}\left[1 - m_\rho^{(n)}(\rho)\sin\left(\beta_{sw}\rho - k\,\hat{\mathbf{r}}_n\cdot\boldsymbol{\rho} + \Phi_\rho^{(n)}\right)\right] \quad (5)\\
m_\chi^{(n)}(\rho) &= m(\rho)\left|\mathbf{e}_n\cdot\hat{\boldsymbol{\chi}}\right|\\
\Phi_\chi^{(n)} &= \tan^{-1}\left[\mathrm{Im}\left(\mathbf{e}_n\cdot\hat{\boldsymbol{\chi}}\right)/\mathrm{Re}\left(\mathbf{e}_n\cdot\hat{\boldsymbol{\chi}}\right)\right] \qquad \chi = \rho,\varphi
\end{aligned}$$

where β_{sw} is the radial wavenumber of the SW excited by a VED on a MTS with surface reactance X_0, namely, the average impedance in (5) [2]. In all the examples, $\beta_{sw}/k = 1.38$. The normalized modulation function $m(\rho)$ has been obtained as in [4], to increase the aperture efficiency. The modulated reactance tensor in (4) has been simulated with the MoM code in [12]. Fig. 2(a) and (b) present the obtained RHCP and left-handed circularly polarized (LHCP) components of the far-fields in the (u,v) plane, where $u = \sin\theta\cos\varphi$ and $u = \sin\theta\sin\varphi$ are the cosine direction of the principal axis. Each beam presents a 28.8 dBi gain, and the maximum cross-polar (X-Pol) level is 12.3 dBi.

B. Case B): single source with aperture sharing

Now, instead of dividing the aperture in independent angular sectors, the individual modulation patterns for every beam are added up at each point of the aperture. Namely, the transparent surface impedance tensor reads as

$$\underline{\underline{\mathbf{X}}} = \frac{1}{2}\sum_{n=1}^{2}\left(\hat{\boldsymbol{\rho}}\hat{\boldsymbol{\rho}}\, X_{\rho\rho}^{(n)} + \left(\hat{\boldsymbol{\rho}}\hat{\boldsymbol{\varphi}} + \hat{\boldsymbol{\varphi}}\hat{\boldsymbol{\rho}}\right) X_{\rho\varphi}^{(n)} + \hat{\boldsymbol{\varphi}}\hat{\boldsymbol{\varphi}}\, X_{\varphi\varphi}^{(n)}\right) U_A \quad (6)$$

where the components of the tensor are defined as in (5). The difference between (5) and (6) is that in (6) the partition function U_n is omitted, i.e., the four elliptical modulation patterns coexist on the same aperture. The results for the MoM simulation of the reactance tensor in (6) are shown in Fig. 3(a) and (b), which show the RHCP and LHCP far-fields, respectively. In this case, the beams' gain is 31.5 dBi and the maximum X-Pol level 12.6 dBi.

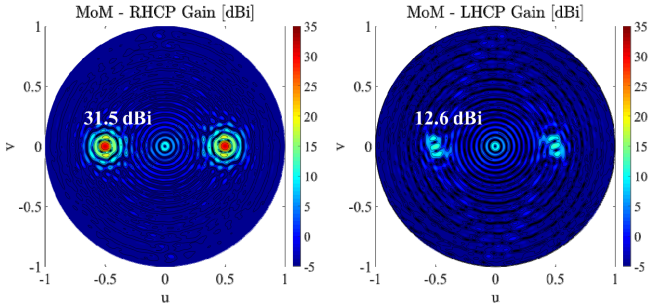

Fig. 3. (a) RHCP and (b) LHCPs gain in the *u-v* plane for the reactance tensor given by (6).

C. Case C): multiple sources with aperture sharing

The main difference with respect to (6) is that each $X^{(n)}$ will be referred to a local coordinate system centered at its corresponding feeding point. Hence, the observation point in the aperture plane will be given by $\mathbf{R}_n = \boldsymbol{\rho} - \boldsymbol{\rho}_n$, where $\boldsymbol{\rho}_n$ is the position vector of the *n*-th source. The unit vectors centered at the sources are

$$\hat{\boldsymbol{\kappa}}_n = \left(\boldsymbol{\rho} - \boldsymbol{\rho}_n\right) / R_n, \;\; \hat{\boldsymbol{\gamma}}_n = \left(\hat{\mathbf{z}} \times \hat{\boldsymbol{\kappa}}_n\right) \quad (7)$$

where $R_n = \left|\boldsymbol{\rho} - \boldsymbol{\rho}_n\right|$, and the surface reactance tensor can be written as

$$\underline{\underline{\mathbf{X}}} = \frac{1}{2}\sum_{n=1}^{2}\left(\hat{\boldsymbol{\kappa}}_n\hat{\boldsymbol{\kappa}}_n X_{\kappa\kappa}^{(n)} + \left(\hat{\boldsymbol{\kappa}}_n\hat{\boldsymbol{\gamma}}_n + \hat{\boldsymbol{\gamma}}_n\hat{\boldsymbol{\kappa}}_n\right) X_{\kappa\gamma}^{(n)} + \hat{\boldsymbol{\varphi}}_n\hat{\boldsymbol{\varphi}}_n X_{\gamma\gamma}^{(n)}\right) U_A \quad (8)$$

where the expressions for $X_{\kappa\kappa}^{(n)}, X_{\kappa\gamma}^{(n)}, X_{\gamma\gamma}^{(n)}$ can be obtained from (5) by formal substitution of the subscripts ρ, φ by κ, γ, respectively.

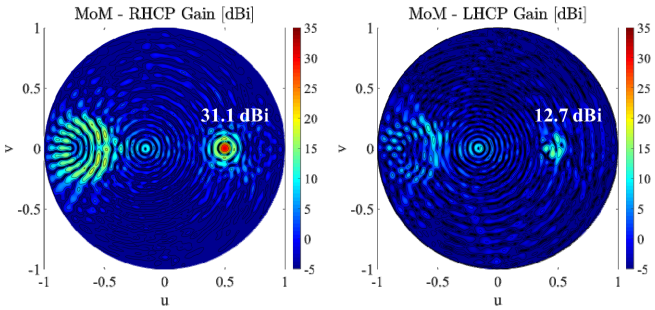

Fig. 4. (a) RHCP and (b) LHCPs gain in the *u-v* plane for the reactance tensor given by (8).

Fig. 4(a) and (b) show the *u-v* plane RHCP and LHCP far-fields, respectively, obtained by exciting the VED located at $\boldsymbol{\rho}_1 = 1.375\lambda\hat{\mathbf{x}}$, whereas the other source is passively terminated. With this configuration, we obtain one beam with 31.1 dBi gain, and X-Pol levels below 12.7 dBi.

III. CONCLUSIONS

Next, we will discuss the performance of the three solutions. To that end, the "beam efficiency" is defined as the quantity $\varepsilon_b = NG/[\cos\theta_0 (ka)^2]$, where $N=2$ (number of beams) and $\cos\theta_0 (ka)^2$ is the maximum gain provided in the direction θ_0 by a uniformly illuminated circular aperture of radius a. For case A) in Fig. 2, we have $\varepsilon_b = 30.8\%$, while with case B) one obtains $\varepsilon_b = 57.4\%$. This is expected, given that in case B) each beam is formed by the entire aperture instead of by just one sector. Finally, in case C) one has $\varepsilon_b = 52.3\%$. As opposed to the single-source case A) and B), independent control of the beams is obtained by introducing multiple sources. By exciting each source one will activate one beam at a time. The produced beams are quasi-orthogonal, which offers a significant advantage for processing signals impinging from different directions. Applications of the antennas presented here are found in Doppler radio-guides and radio altimeters.

IV. ACKNOWLEDGEMENTS

This work has been carried out at the Jet Propulsion Laboratory, California Institute of Technology, under a contract with National Aeronautics and Space Administration (NASA).

The work of D. Gonzalez-Ovejero was supported by a Marie Curie International Outgoing Fellowship within the 7th European Community Framework Programme. The work of G. Minatti, E. Martini and S. Maci has been supported by the European Space Agency (ESA-ESTEC, Noordwijk, The Netherlands) under contract 4000111496/14/NL/GLC/al "Low Complexity Data Downlink Antenna" and by the Army Research Laboratory under contract No. W911NF-15-1-0528.

REFERENCES

[1] B. H. Fong, J. S. Colburn, J. J. Ottusch, J. L Visher, and D. F. Sievenpiper, "Scalar and tensor holographic artificial impedance surfaces," *IEEE Trans. Antennas Propag.*, vol. 58, no. 10, pp. 3212–3221, Oct. 2010.

[2] G. Minatti, M. Faenzi, E. Martini, F. Caminita, P. De Vita, D. González-Ovejero, M. Sabbadini, and S. Maci, "Modulated metasurface antennas for space: Synthesis, analysis and realizations," *IEEE Trans. Antennas Propag.*, vol. 63, no. 4, pp. 1288–1300, Apr. 2015.

[3] S. Pandi, C. A. Balanis and C. R. Birtcher, "Design of scalar impedance holographic metasurfaces for antenna beam formation with desired polarization," *IEEE Trans. Antennas Propag.*, vol. 63, no. 7, pp. 3016-3024, Jul. 2015.

[4] G. Minatti, F. Caminita, E. Martini, M. Sabbadini, and S. Maci, "Synthesis of modulated-metasurface antennas with amplitude, phase and polarization control," *IEEE Trans. Antennas Propag.*, vol. 64, no. 9, pp. 3907-3919, Sept. 2016. .

[5] D. González-Ovejero, T. J. Reck, C. D. Jung-Kubiak, M. Alonso-DelPino, and G. Chattopadhyay, "A class of silicon micromachined metasurface for the design of high-gain terahertz antennas," in *Proc. IEEE AP-S Soc. Int. Symp.*, Fajardo, PR, 2016.

[6] D. González-Ovejero, G. Chattopadhyay, and S. Maci, "Multiple beam shared aperture modulated metasurface antennas" in *Proc. IEEE AP-S Soc. Int. Symp.*, Fajardo PR, Jul. 2016.

[7] Y.B. Li, X. Wan, B.G. Cai, Q. Cheng, T.J. Cui, "Frequency-controls of electromagnetic multi-beam scanning by metasurfaces", Scientific Reports, Vol 4: 6921, 5 November 2014.

[8] E. F. Kuester, M. Mohamed, M. Piket-May, and C. Holloway, "Averaged transition conditions for electromagnetic fields at a metafilm," *IEEE Trans. Antennas Propag.*, vol. 51, no. 10, pp. 2641–2651, Oct. 2003

[9] C. Holloway, E. F. Kuester, J. Gordon, J. O'Hara, J. Booth, and D. Smith, "An overview of the theory and applications of metasurfaces: The two-dimensional equivalents of metamaterials," *IEEE Antennas Propag. Mag.*, vol. 54, no. 2, pp. 10–35, Apr. 2012.

[10] G. Minatti, F. Caminita, E. Martini, and S. Maci, "Flat optics for leaky-waves on modulated metasurfaces: adiabatic Floquet-wave analysis," *IEEE Trans. Antennas Propag.*, vol. 64, no. 9, pp. 3896-3906, Sept. 2016.

[11] M. Mencagli Jr., E. Martini, and S. Maci, "Surface wave dispersion for anisotropic metasurfaces constituted by Elliptical Patches," *IEEE Trans. Antennas Propag.*, vol. 63, no. 7, pp. 2992-3003, Jul. 2015.

[12] D. González-Ovejero and S. Maci, "Gaussian ring basis functions for the analysis of modulated metasurface antennas," *IEEE Trans. Antennas Propag.*, vol. 63, no. 9, pp. 3982–3993, Sep. 2015.

[13] D. González-Ovejero, G. Minatti, G. Chattopadhyay and S. Maci, "Multibeam by Metasurface Antennas," *IEEE Trans. Antennas Propag.*, submitted.